Biogeosciences Discuss., 12, 14441–14479, 2015
www.biogeosciences-discuss.net/12/14441/2015/
doi:10.5194/bgd-12-14441-2015

Biogeosciences Discussions
Open Access

Box-modeling of the impacts of atmospheric nitrogen deposition and benthic remineralization on the nitrogen cycle of the eastern tropical South Pacific

B. Su, M. Pahlow, and A. Oschlies

GEOMAR Helmholtz-Zentrum für Ozeanforschung Kiel, Marine Biogeochemical Modelling, Düsternbrooker Weg 20, 24105 Kiel, Germany.

Received: 25 April 2015 – Accepted: 20 May 2015 – Published: 2 September 2015

Correspondence to: B. Su (bsu@geomar.de)

Published by Copernicus Publications on behalf of the European Geosciences Union.

Abstract

Both atmospheric deposition and benthic remineralization influence the marine nitrogen cycle, and hence ultimately also marine primary production. The biological and biogeochemical relations of the eastern tropical South Pacific (ETSP) to nitrogen deposition, benthic denitrification and phosphate regeneration are analysed in a prognostic box model of the oxygen, nitrogen and phosphorus cycles in the ETSP. In the model, atmospheric nitrogen deposition based on estimates for the years 2000–2009 is offset by half by reduced N_2 fixation, with the other half transported out of the model domain. Both model- and data-based benthic denitrification are found to trigger nitrogen fixation, partly compensating for the NO_3^- loss. Since phosphate is the ultimate limiting nutrient in the model, enhanced sedimentary phosphate regeneration under suboxic conditions stimulates primary production and subsequent export production and NO_3^- loss in the oxygen minimum zone (OMZ). A sensitivity analysis of the local response to both atmospheric deposition and benthic remineralization indicates dominant stabilizing feedbacks in the ETSP, which tend to keep a balanced nitrogen inventory, i.e., nitrogen input by atmospheric deposition is counteracted by decreasing nitrogen fixation; NO_3^- loss via benthic denitrification is partly compensated by increased nitrogen fixation; enhanced nitrogen fixation stimulated by phosphate regeneration is partly removed by the stronger water-column denitrification. Even though the water column in our model domain acts as a NO_3^- source, the ETSP including benthic denitrification might become a NO_3^- sink.

1 Introduction

Marine primary production (PP) by phytoplankton is a key factor controlling the strength of the oceanic biological carbon pump and the amount of CO_2 that is stored in the ocean (Gruber, 2004; Okin et al., 2011). PP is controlled by light and nutrients, such as nitrogen, phosphorus or iron, necessary for the production of phytoplankton. These

BGD
12, 14441–14479, 2015

nutrients are supplied to the light-lit surface waters by upwelling, turbulent entrainment of subsurface water, riverine inputs, biological nitrogen fixation, atmospheric deposition and benthic remineralisation (Falkowski et al., 1998; Kasai et al., 2002; Duce et al., 2008; Bakun and Weeks, 2008; Moore and Braucher, 2008).

Nitrogen is often the limiting nutrient for phytoplankton in the ocean (Moore et al., 2013). On the other hand, oceanic nitrogen is thought to adjust, via nitrogen gain and loss processes, to the marine phosphorus inventory on geological time scales, making phosphorus the ultimate limiting nutrient and nitrogen the proximate limiting nutrient (Tyrrell, 1999). The ocean's nitrogen inventory has a turnover time of a few thousand years, being affected by relatively large interacting nitrogen sinks and sources. The exact mechanisms and timescales of the interactions are not well understood. Estimates of oceanic nitrogen fixation, the main fixed-N source into the ocean, vary from 106 to 330 $\mathrm{Tg\,N\,yr^{-1}}$ based on both in-situ observations and models (Codispoti et al., 2001; Brandes and Devol, 2002; Gruber and Sarmiento, 2002; Gruber, 2004; Großkopf et al., 2012). Water-column denitrification and anaerobic ammonium oxidation (anammox) in oxygen minimum zones (OMZs), accounting for 100–300 $\mathrm{Tg\,N\,yr^{-1}}$, and benthic denitrification, estimated as 95–300 $\mathrm{Tg\,N\,yr^{-1}}$, mainly determine the oceanic fixed-N sink (Gruber and Sarmiento, 2002; Gruber, 2004; Codispoti, 2007; Bohlen et al., 2012; Eugster and Gruber, 2012; DeVries et al., 2012). Due to the large uncertainty in the major sources and sinks of the global nitrogen cycle, the balance of the nitrogen inventory in the ocean is still a matter of debate (Gruber, 2004; Codispoti, 2007; DeVries et al., 2012).

Phosphate can be the ultimate limiting nutrient on geological time scales even in regions with fixed nitrogen deficits with respect to the Redfield-equivalent of the phosphate concentration (Tyrrell, 1999; Su et al., 2015; Auguéres and Loreau, 2015). The ocean's phosphorus budget has been suggested to be unbalanced in the modern ocean with sedimentary burial as the major sink exceeding phosphorus sources (Wallmann, 2010). This condition might be alleviated by benthic phosphate regeneration, which can be enhanced under low-oxygen bottom waters ($O_2 < 20\,\mu\mathrm{mol\,L^{-1}}$) (Slomp

BGD
12, 14441–14479, 2015

and Van Cappellen, 2007; Wallmann, 2010). Input of bioavailable phosphorus into the ocean stimulates primary production, and decomposition of subsequent export production enhances O_2 consumption in the ocean, in turn increasing the volume of oceanic oxygen-deficit water and the fixed-N loss. Consequently, phosphate regeneration is expected to be enhanced by enlarging OMZs, possibly leading to a positive feedback loop (Van Cappellen and Ingall, 1994; Wallmann, 2003).

OMZs also play an important role in the global marine fixed-N budget as they are responsible for a large fraction of total marine fixed-N loss (Canfield, 2006). The relative contribution of heterotrophic denitrification and autotrophic anammox to the total oceanic fixed-nitrogen sink remains debated (Lam et al., 2009; Ward et al., 2009). Even though anammox has been observed to be a major fixed-N loss in the eastern tropical South Pacific (ETSP) (Lam et al., 2009; Kalvelage et al., 2013), both denitrification and anammox are ultimately driven by the flux of organic matter into the OMZ (Koeve and Kähler, 2010; Kalvelage et al., 2013). For simplicity, heterotrophic denitrification is considered the major fixed-N loss process in the present study. Continental shelves and the upper continental slopes are the most important sites for benthic fixed-N loss (Christensen et al., 1987; Devol, 1991). However, Bohlen et al. (2011) found that the continental shelf and upper continental slope of the ETSP across a section at 11° S are sites of nitrogen recycling rather than fixed-N loss, because of relatively low rates of denitrification and high rates of NH_4^+ release from Dissimilatory Nitrate Reduction to Ammonium (DNRA). This illustrates that the NH_4^+ released from DNRA should be taken into account when the benthic fixed-N sink is estimated.

In the last few decades, a number of model and data based investigations have been carried out on the importance of atmospheric fixed-N input into the ocean for marine biogeochemical cycles (Duce, 1986; Duce et al., 1991; Krishnamurthy et al., 2007, 2010; Okin et al., 2011; Mouriño-Carballido et al., 2012). Duce et al. (2008) indicate that anthropogenic nitrogen deposition is rapidly approaching the global oceanic estimates for N_2 fixation, while preindustrial deposition was an order of magnitude lower than N_2 fixation. However, the response of nitrogen-fixation and denitrification to at-

BGD
12, 14441–14479, 2015

mospheric nitrogen deposition remains an open question. Atmospheric nitrogen inputs into the global ocean are dominated by inorganic nitrogen from anthropogenic sources (Warneck, 1988; Paerl and Whitall, 1999). The exact magnitude of organic nitrogen deposition is not clear due to a lack of observations (Cornella et al., 2003; Duce et al., 2008; Zamora et al., 2011). Thus, the contribution of DON to total nitrogen deposition is still uncertain and the distribution, bioavailability and lifetime are also not clear (Seitzinger and Sanders, 1999; Duarte et al., 2006; Duce et al., 2008). Therefore, DON deposition is excluded from our analysis.

Various biogeochemical models have addressed the effects and feedbacks between the major sources and sinks in the marine nitrogen cycle (Van Cappellen and Ingall, 1994; Deutsch et al., 2001, 2007; Krishnamurthy et al., 2007; Somes et al., 2013; Landolfi et al., 2013). However, most of them have explored only a subset of the atmospheric, pelagic and benthic nitrogen sources and sinks. Using a conceptually simple and computationally efficient box model, we here attempt a synthesis considering all essential sources and sinks and their mutual interactions, with the only exception of riverine input, which is excluded from our model analysis because of its unknown and presumably minor role in the ETSP.

2 Model description

2.1 Circulation and biogeochemical model

The circulation model is the same as in Su et al. (2015), which is a prognostic 5-box model to explore the interactions among oceanic circulation, nitrogen fixation and water-column denitrification in the OMZ of the ETSP. Briefly, the physical parameters were calibrated to fit the average $\delta^{14}C$ of each box and biogeochemical parameters are constrained by literature data. All the simulations in this manuscript employ the Open-boundary + Reduced-denitrification (OBRD) configuration of Su et al. (2015), which allows for exchange of deep and intermediate ETSP waters with the Southern Ocean

BGD
12, 14441–14479, 2015

("SO" in Fig. 1) and applies reduced remineralisation rates under suboxic conditions. The model domain consists of five boxes representing the water column of an upwelling region and an adjacent ocean basin. The U box represents the upper upwelling region. The UM box is the OMZ below, where suboxia is expected to develop. The S box represents the surface ocean away from the upwelling zone. Below the S box sits the I box, which represents water of intermediate depth and exchanges water with UM. D is the deep box, which represents water deeper than 500 m (model configuration shown in Fig. 1).

There are two phytoplankton types in the biogeochemical model, ordinary phytoplankton, Phy, and nitrogen fixers, NF, as defined in Su et al. (2015). Both Phy and NF require phosphate, whereas nitrate is required in addition to phosphate only by Phy, and NF can fix N_2 as long as PO_4^{3-} is available. Dead phytoplankton is immediately remineralized in the surface layer and underlying boxes according to the pre-defined remineralization fractions. Remineralization occurs preferentially via aerobic respiration, with anaerobic denitrification and the associated nitrogen loss setting in only when all O_2 has been consumed by aerobic respiration. When oxygen is exhausted in the OMZ, remineralization is assumed to slow down by a factor of 5, and accordingly denitrification within the UM box is responsible for 1/5 of the remaining organic matter remineralization and the remainder will be remineralized in the D box.

In order to represent the nitrogen and phosphate fluxes across the water–sediment interface, remineralization of particulate organic carbon reaching the sediment (POC rain rate, RRPOC) is included additionally in the UM and D boxes. RRPOC is calculated according to the method introduced in Sect. 2.4, and we assume that all the POC is buried in the sediment.

2.2 Model configurations

The above descriptions define the control configuration. In order to investigate the model sensitivity to atmospheric nitrogen deposition and benthic remineralization, we employ another nine model configurations incorporating either a subset or all of these

BGD
12, 14441–14479, 2015

processes, which are summarized in Table 1. Detailed information of all processes is presented in Sects. 2.3, 2.4 and 2.5.

2.3 Atmospheric nitrogen deposition

Years 2000–2009 levels of dry and wet inorganic nitrogen deposition following the RCP 4.5 scenario (Lamarque et al., 2011) are examined in our work. Inferred atmospheric inorganic nitrogen deposition rates are 0.081 and 1.4 $\mathrm{Tg\,N\,yr^{-1}}$ (73.1 and 64.9 $\mathrm{mg\,N\,m^{-2}\,yr^{-1}}$) for the U and S box, respectively. Note that the circulation remains constant in our model, and only atmospheric nitrogen deposition fluxes are included as an additional annual nitrogen input into the surface (U and S) boxes.

Duce et al. (1991) estimated atmospheric dissolved inorganic phosphorus (DIP) input into the global ocean, which indicates high N/P (mole/mole) ratios of more than 100 on a global scale (Dentener et al., 2006; Duce et al., 2008; Mahowald et al., 2008), much higher than the average elemental N/P required by phytoplankton in the ocean. Thus, we do not explore the influence of atmospheric phosphorus deposition in our analysis.

2.4 Benthic denitrification

The empirical transfer function of Bohlen et al. (2012) is applied to predict benthic inorganic nitrogen loss (L_{DIN} in $\mathrm{\mu mol\,N\,m^{-2}\,d^{-1}}$) through benthic denitrification, which can account for the net loss of dissolved inorganic nitrogen (DIN) from the sediment.

$$L_{\mathrm{DIN}} = (0.06 + 0.19 \cdot 0.99^{(O_2 - NO_3^-)_{\mathrm{bw}}}) \cdot \mathrm{RRPOC} \quad (1)$$

where NO_3^- and O_2 are bottom-water nitrate and oxygen concentrations in $\mathrm{\mu mol\,kg^{-1}}$, and the rain rate (RRPOC) is in $\mathrm{\mu mol\,C\,m^{-2}\,d^{-1}}$. Since the bottom-water NO_3^- and O_2 concentrations are well known in the ETSP, the uncertainty in our estimation of benthic denitrification comes mostly from uncertainties in the rain rate, which, in turn, depends

BGD
12, 14441–14479, 2015

on biological production, as a function of phytoplankton biomass and its physiological status. Simulated phytoplankton concentrations in the surface boxes of the model roughly agree with estimates by Behrenfeld et al. (2005) from Aqua-Modis satellite data and the Redfield C : N ratio (U-box: 1.06 $\mu mol\,N\,kg^{-1}$ simulated vs. 0.68 $\mu mol\,N\,kg^{-1}$ from Aqua-Modis; S-Box: 0.23 $\mu mol\,N\,kg^{-1}$ simulated vs. 0.28 $\mu mol\,N\,kg^{-1}$ from Aqua-Modis).

2.4.1 Model-based estimation of benthic denitrification

Fixed-N losses via benthic denitrification (L_{DIN}) in the UM and D boxes are obtained according to Eq. (1), with the respective simulated actual NO_3^- and O_2 concentrations taken as the bottom-water concentrations, and RRPOC is estimated from the export production out of the U and S boxes (EP_U and EP_S) and the Martin curve (Eq. 2) (Martin et al., 1987):

$$RRPOC = F \cdot \left(\frac{z}{100}\right)^{-b} \quad (2)$$

where RRPOC is the rain rate, F is the export production from both surface boxes, and z is the water depth. The bathymetry of the regions of the UM and D boxes is derived from ETOPO2 (http://www.ngdc.noaa.gov/mgg/gdas/gd_designagrid.html). We apply $b = 0.82$ in Eq. (2), which is the global average according to Berelson (2001) and also close to his estimate for the ETSP. An exponent of 0.4 for Eq. (2) in suboxic water is implied by Van Mooy et al. (2002). Therefore, sensitivity experiments are performed with $b = 0.4$. From Eq. (2) and the fraction of the lower boundary of the respective box in contact with the seafloor, the RRPOC at the sediment surfaces of the UM and D boxes is calculated according to Eqs. (3) and (4):

$$RRPOC_{UM} = EP_U \cdot SD_{UM} \cdot AMC_{UM} \quad (3)$$

$$RRPOC_D = (EP_U + EP_S) \cdot SD_D \cdot AMC_D \quad (4)$$

BGD
12, 14441–14479, 2015

where AMC_{UM} and AMC_D are the average Martin-curve values corresponding to the actual water depth (z) in the grid of ETOPO2 respectively; SD_{UM} and SD_D represent the percentages in contact with the sediment in the UM and D boxes (Table 2).

2.4.2 Data-based estimation of benthic denitrification

For a second and independent estimate of L_{DIN}, we combine observations from different datasets. O_2 and NO_3^- concentrations for our model domain are obtained from the annual objectively analyzed mean concentrations of the WOA 2009 $1^\circ \times 1^\circ$ data (Garcia et al., 2010a, b), and interpolated over the region of our model domain to match the resolutions of the other datasets.

RRPOC is estimated from primary production following Bohlen et al. (2012). According to the carbon-based approach of Behrenfeld et al. (2005), average annual primary production is derived from photosynthetically available radiation (PAR), the diffuse attenuation coefficient at 490 nm (K490), chlorophyll *a* (Chl *a*) and mixed layer depth (MLD). PAR, K490 and Chl *a* are from the Aqua-Modis satellite data (2005–2010) (http://oceancolor.gsfc.nasa.gov/), and MLD is from the Hybrid Coordinate Ocean Model (HYCOM, http://orca.science.oregonstate.edu/1080.by.2160.monthly.hdf.mld.hycom.php) Export production is estimated from primary production and sea-surface-temperature (SST) (Dunne et al., 2005), where SST is from the WOA 2009 annual average $1^\circ \times 1^\circ$ temperature data (Locarnini et al., 2010). The rate of particle transport at each grid cell to the seafloor is calculated using the Martin curve (Eq. 2) (Martin et al., 1987). To obtain more accurate estimates for RRPOC of our regional box model, all data processed in this experiment are interpolated on a grid of $2' \times 2'$ in the UM box and $20' \times 20'$ in the D box, and the ETOPO2 data ($2' \times 2'$) are averaged within each $20' \times 20'$ grid cell in the D box. The Aqua-Modis data ($5' \times 5'$) and NO_3^- and O_2 concentrations from WOA 2009 dataset are interpolated or averaged horizontally to match these resolutions. The vertical resolution of the NO_3^- and O_2 concentrations are interpolated to resolve the bathymetry of the ETOPO2 data, and the NO_3^- and O_2

BGD
12, 14441–14479, 2015

concentrations closest to the sediment are applied in Eq. (1) for the bottom water NO_3^- and O_2 concentrations.

Finally, the L_{DIN} derived from observational datasets are averaged over the regions represented by UM and D boxes to produce an annual NO_3^- loss term.

2.5 Phosphate regeneration

Phosphate regeneration is estimated according to Wallmann (2010) and Flögel et al. (2011) with both model- and data-based estimates for the rain rate. We estimate benthic PO_4^{3-} regeneration (resupply of benthic PO_4^{3-} into the water column, Ben_{DP}) from the RRPOC degradation ratio (r_{REG}) and the POC burial rate in the sediments (BURPOC) according to:

$$Ben_{DPUM} = \frac{RRPOC_{UM} - BURPOC_{UM}}{r_{REG}} \quad (5)$$

$$Ben_{DPD} = \min\left(\frac{RRPOC_D - BURPOC_D}{r_{REG}}, \frac{RRPOC}{106}\right) \quad (6)$$

where RRPOC is estimated with the methods described in Sects. 2.4.1 and 2.4.2. A minimum condition is introduced in the D-box to prevent Ben_{DP} exceeding the rain rate of particulate organic phosphate (RRPOP = RRPOC / 106) to the deep ocean, but not for the UM box, because there are possible extra sources of RRPOP, such as inputs via weathering or eolian deposition, onto the continental shelf, which is contained in the UM box in our model.

BURPOC is estimated from Eq. (7) for the continental shelf (UM box) and Eq. (8) for the deep-sea sediment (D box), and r_{REG} is the C : P regeneration ratio estimated via

BGD
12, 14441–14479, 2015

Eq. (9) following the empirical relations of Wallmann (2010).

$$BURPOC_{UM} = 0.14 \cdot RRPOC_{UM}^{1.11} \quad (7)$$

$$BURPOC_{D} = 0.014 \cdot RRPOC_{D}^{1.05} \quad (8)$$

$$r_{REG} = 123 + (-112) \cdot \exp\left(-\frac{O_2}{32}\right) \quad (9)$$

where O_2 is the oxygen concentration in the ambient bottom water (in $\mu mol\,kg^{-1}$). r_{REG} in Eq. (9) is higher than the Redfield ratio in oxic water, resulting in preferential P burial under oxic conditions; it is much smaller than the Redfield ratio when $O_2 < 20\,\mu mol\,kg^{-1}$, indicating excess phosphate release from the sediment under suboxic conditions.

2.6 Synthesis configurations

Nitrogen deposition, benthic denitrification and phosphate regeneration are integrated into the synthesis model configurations to explore the model sensitivity to each process and their mutual interactions in the ETSP. The configurations (Syn1 to Syn4) with different benthic processes and atmospheric inputs are summarized in Table 1.

2.7 Model sensitivity experiments

Since our model domain only includes the top 2000 m of the water column, the sediments only account for a small portion of the whole sediment of the ETSP (Table. 2). A sensitivity experiment is performed with the assumption that all of the bottom of the D box is in contact with the sediment below 500 m (high benthic denitrification (high-BD), or high phosphate regeneration (high-PR)) including all NO_3^- losses by benthic denitrification and phosphate release by phosphate regeneration of the sediment.

The original work of Martin et al. (1987) and Van Mooy et al. (2002) indicate a lower value for the exponent b of Eq. (2) in suboxic water. We perform an additional sensitivity experiment with $b = 0.4$ according to the suggestion by Van Mooy et al. (2002),

BGD
12, 14441–14479, 2015

to explore the influence of benthic denitrification and phosphate regeneration under conditions of slower POC remineralization.

3 Results

3.1 Nitrogen deposition

Due to the low NO_3^- concentrations in the surface U and S boxes, the annual nitrogen input by atmospheric nitrogen deposition accounts for 63 and 10 %, respectively, of nitrogen inventories of the U and S boxes. Figure 2 indicates that the extra fixed-N input by nitrogen deposition reduces the growth of nitrogen fixers in the surface ocean by about 0.72–0.73 Tg N yr^{-1} (about 12 % of total nitrogen fixation), which accounts for about 48 % of the total fixed-N inputs into surface waters from atmospheric deposition (1.5 Tg N yr^{-1}). Water-column denitrification stays almost unchanged because the increase in export production (EP) of Phy is almost exactly compensated by the decrease in EP of NF, resulting in essentially unchanged total EP. As a result of the ~ 50 % of the nitrogen deposition not immediately compensated by a decline in nitrogen fixation, the model domain becomes a larger fixed-N source (Fig. 2). The N-loss through the lateral boundary increases from 0.93 Tg N yr^{-1} in the control configuration to 1.7 Tg N yr^{-1} in the configurations including nitrogen deposition, leading to about 0.78 Tg N yr^{-1} extra fixed-N loss from the model domain, i.e. about 50 % of the total fixed-N input by nitrogen deposition. Thus, almost all the extra nitrogen input into the model domain via nitrogen deposition is offset by lower nitrogen fixation and nitrogen loss by lateral transport out of the model domain.

There is no significant influence of nitrogen deposition on the biogeochemical tracer concentrations of the model at steady state: ordinary phytoplankton (Phy) concentrations increase by 3 % in the U box and even smaller changes occur in the S box, which can be attributed to the stronger nitrogen deficit in the region above the OMZ (U box) than in the open ocean (S box) (not shown). Largest changes are found for the concen-

BGD
12, 14441–14479, 2015

tration of nitrogen fixers (NF) that decrease by about 9 % in the U box, counteracting the nitrogen input via nitrogen deposition (Fig. 3). Again in the S box, NF concentration stays almost unaltered (Fig. 3). There are also slight variations of the NO_3^- concentration in the UM box and of the O_2 concentrations in the I and D boxes (not shown).

3.2 Benthic denitrification

The data-derived benthic denitrification and phosphate regeneration in the UM and D boxes are shown in Table 3. The modeled net primary production (NPP) in the surface ocean above the UM and D boxes is, respectively, 1.4 and 0.87 $g C m^{-2} day^{-1}$, indicating higher NPP in the coastal upwelling region and lower NPP in the open ocean adjacent to the upwelling region, which is consistent with the estimate by Behrenfeld et al. (2005). Due to the small sediment area percentages, the annual nitrogen loss by benthic denitrification is 0.17 and 0.82 $Tg N yr^{-1}$ in the UM and D boxes, accounting for only about 0.14 % and 5.1×10^{-3} % $year^{-1}$, respectively, of the NO_3^- inventories (Table 3). The higher sedimentary NO_3^- sink in the UM box can be attributed to the anoxic conditions and larger RRPOC there.

Our simulated biogeochemical tracer concentrations at steady state are quite robust with respect to including benthic denitrification (Fig. 3). There are only minor deviations of the MBD and DBD configurations from the control run. Nitrogen fixation rates increases by about 2.9 and 5.8 % respectively in the MBD and DBD configurations (A-bars in panels MBD and DBD of Fig. 4). Obviously, the response is stronger in the DBD configuration than in the MBD configuration, because there is an approximately 5-times larger fixed-N loss via benthic denitrification in the DBD configuration (A-bars in Fig. 4). The DBD configuration results in stronger responses of nitrogen fixation and lateral fluxes to benthic denitrification: the increase in nitrogen fixation can not fully compensate the nitrogen loss by benthic denitrification, thus, the model domain becomes a smaller fixed-N source, about 25 % of that in the control configuration. Otherwise, the steady-state solutions of the MBD and DBD configurations are almost identical to that of the control configuration after including benthic denitrification. The

BGD
12, 14441–14479, 2015

temporal development of biogeochemical tracer concentrations is also insensitive to including benthic denitrification (not shown).

3.3 Phosphate regeneration

Phosphate release by phosphate regeneration accounts for about 0.23 % and 2.2×10^{-3} % year^{-1}, respectively, of the total phosphate inventories in the UM and D boxes (Table 2). The higher sedimentary PO_4^{3-} source in the UM box can be attributed to the anoxic conditions and larger RRPOC there. The phosphate release associated with benthic phosphate regeneration can stimulate nitrogen fixation and EP from the surface ocean, followed by higher water-column denitrification, owing to enhanced decomposition of exported organic matter (A-bars in MPR and DPR panels of Fig. 4). In the MPR configuration, nitrogen fixation and water-column denitrification increase by 12 and 11 %, respectively, while in the DPR configuration, nitrogen fixation and water-column denitrification increase by about 17 and 15 % (A-bars in MPR and DPR panels of Fig. 4). Compared with the MBD and DBD configurations, phosphate regeneration cannot turn our model domain into a smaller fixed-N source even though there is higher water-column denitrification, because nitrogen fixation can compensate for the nitrogen loss by water-column denitrification (A-bars in Fig. 4).

While changes in nitrogen deposition and benthic denitrification are to a large extent compensated by adjustments via simulated nitrogen fixation, phosphate is the ultimate limiting nutrient in our model domain (Su et al., 2015). Hence the extra phosphate input into the model domain by phosphate regeneration has a more significant influence on the steady-state model results than the perturbations of the nitrogen input or loss applied in the model (Fig. 3). Phy concentration in the DPR configuration decreases in the U box but remains unchanged in the S box (not shown). Phy concentrations in the U and S boxes remain almost unaltered in the MPR configuration. Compared with the control configuration, NF concentrations in the U and S boxes increase by 11 and 1.6 % respectively in the MPR configuration, and 14 and 1.6 % respectively in the DPR configuration (Fig. 3). The nitrate concentration in the UM box decreases by

BGD
12, 14441–14479, 2015

about 3.8 % in the MPR configuration and 5.2 % in the DPR configuration (not shown). The temporal development of biogeochemical tracer concentrations is also robust to benthic phosphate regeneration (not shown).

3.4 Synthesis configurations

In the synthesis configurations (Table 1), phytoplankton, nutrient and oxygen concentrations are quite robust with respect to the various fluxes associated with nitrogen input or removal and phosphate release from the sediment into the water column (Fig. 3). However, the interactions among nitrogen fixation, water-column denitrification, benthic denitrification, and phosphate regeneration result in different sensitivities of nitrogen fixation and the lateral flux to atmospheric N deposition in the presence of benthic denitrification and phosphate regeneration (Fig. 3). In contrast to the N-DEP configuration, nitrogen fixation rates in the Syn3 and Syn4 configurations increase by about 1.7 and 8.5 % in spite of additional nitrogen input into model domain by atmospheric nitrogen deposition. The lateral flux out of the model domain (NO_3^- source) increases by about 0.97 $Tg\,N\,yr^{-1}$ in the Syn3 configuration, which accounts for about 65 % of the total nitrogen deposition, so that more than half of the extra nitrogen supplied by nitrogen deposition is not utilised locally. However, in the Syn4 configuration, the lateral NO_3^- efflux increase only accounts for about 25 % of the total nitrogen deposition, with 75 % of the deposited nitrogen utilised in the model domain. Less fixed-N is lost laterally from the model domain in the configurations including data-based estimates than those including model-based estimates, due to more NO_3^- loss within the model domain (Fig. 4). Thus, the lateral fluxes and the sensitivity to nitrogen deposition are also controlled by benthic denitrification and phosphate regeneration rather than nitrogen deposition only.

BGD
12, 14441–14479, 2015

3.5 Model sensitivity

Figure 5 shows the results of the sensitivity experiments with high-BD and high-PR. Compared with Fig. 3, the influence on the biogeochemical tracer concentrations at steady state is stronger, due to the larger NO_3^- loss via benthic denitrification and PO_4^{3-} release via phosphate regeneration (Table 3). High-BD or high-BD together with high-PR can even turn our model domain into a NO_3^- sink (B-bars in panels DBD and DBD+DPR of Fig. 4).

Applying the Martin Curve exponent $b = 0.4$ also amplifies the influence of benthic denitrification and phosphate regeneration on phytoplankton and biogeochemical tracers, although the effect is weaker than in the high-BD and high-PR configurations. For example, NF_U increases by as much as 33 % in the DBD+DPR configuration, and NF_S increase about 15 % (Fig. 6). Compared with A-bars in Fig. 4, this enhanced influence results from the higher NO_3^- loss through benthic denitrification and phosphate input via phosphate regeneration (C-bars in Fig. 4).

Due to the higher RRPOC reaching the sea floor below the water column with suboxic conditions, benthic denitrification increases by about 42 and 198 % (A- and C-bars of panels MBD and DBD in Fig. 4) and phosphate regeneration increases about 36 and 200 % respectively in model- and data-based estimations in the sensitivity experiments with Martin Curve value $b = 0.4$. Our model domain switches to a NO_3^- sink in the DBD and DBD+DPR configurations with $b = 0.4$ (C-bars in Fig. 4). Comparing A- and C-bars of panel DBD in Fig. 4, we find that higher benthic denitrification can stimulate nitrogen fixation, but the water-column denitrification remains constant. However, comparing A- and C-bars of panel DBD+DPR in Fig. 4, we find that higher benthic denitrification can increase nitrogen fixation and water-column denitrification, indicating important role of PO_4^{3-} in the balanced nitrogen inventory. This shows a positive feedback between water-column denitrification in the OMZ and benthic denitrification below, caused by slower remineralisation under 2 anoxic conditions, which results in more RRPOC reaching the sea floor. All above comparisons indicate that phosphate

BGD
12, 14441–14479, 2015

limitation could be responsible for breaking this positive feedback under the assumption of our model that PO_4^{3-} is the only limiting factor for the growth of nitrogen fixers.

4 Discussion and conclusions

The impact of nitrogen deposition on the ETSP has rarely been investigated so far, since this region is believed to receive less atmospheric fixed-N deposition compared with the coasts of western Europe, South and East Asia (Dentener et al., 2006; Duce et al., 2008). The influence of anthropogenic nitrogen deposition on the biogeochemical cycles of the open ocean is increasing and the increase in atmospheric nitrogen deposition will probably induce an approximately 10 % rise in carbon sequestration on land and in the ocean by 2030 (Duce et al., 2008; Reay et al., 2008). The ETSP, a typical N-deficit region due to denitrification in the OMZ, is likely to be sensitive to anthropogenic nitrogen deposition. We find that, in our model, nitrogen deposition can inhibit N_2 fixation by relieving nitrogen limitation for Phy: this counteracts the effect of atmospheric nitrogen input. This is in line with the finding that N_2 fixation decreases with increasing nitrogen deposition in global-scale models that use essentially the same assumptions about the environmental controls on marine nitrogen fixation (Krishnamurthy et al., 2007, 2009, 2010; Zamora et al., 2010). Another portion of the deposited nitrogen is exported out of the model domain since not all the deposited nitrogen can be taken up by Phy locally because of phosphate limitation (Fig. 2). Appendix A shows the model results when there is facultative N_2 fixation, which slightly enhances the strength of the negative feedback between nitrogen fixation and nitrogen deposition.

In a 3-D biogeochemical model study of the nitrogen fixation response to benthic denitrification, Somes et al. (2013) found that an increase of benthic denitrification can stimulate N_2 fixation, but this occurred under the condition that N_2 fixation was tuned to compensate for the fixed-N loss by reducing mortality and predation rates. Nitrogen fixation can also be stimulated by a N-deficit (Deutsch et al., 2007), which can result from benthic denitrification. In our 2-D model, we also find that nitrogen fixation can

BGD
12, 14441–14479, 2015

be enhanced by the N-deficit caused by benthic denitrification, so that nitrogen fixation can somehow compensate for the nitrogen loss.

We find a strong increase in primary production after incorporating benthic phosphate regeneration, which is mainly attributed to nitrogen fixation (Panels MPR and DPR in Fig. 4). Phosphate regeneration will be enhanced under O_2 deficit conditions, and the enhanced phosphate release will stimulate primary production, finally resulting in the expansion of OMZs and a possible positive feedback loop leading to more benthic phosphate regeneration (Van Cappellen and Ingall, 1994; Wallmann, 2010). However, our model domain only represents the upper 2000 m of the ocean and its sediments only account for a small fraction of total sediment in the ETSP. The model results incorporating benthic denitrification and phosphate regeneration for a case where all of the bottom of the D box is assumed in contact with the sediment are shown in Figs. 4 and 5. For our parameterization of nitrogen fixation being favoured in N-deficit waters, the increase of water-column denitrification can always be compensated by increased nitrogen fixation when there is only phosphate regeneration (panels MPR and DPR in Fig. 4). Our model domain can only turn into a fixed-N sink after including high-BD of the full sediment.

Due to the simplicity and computational efficiency of our box model, it is relatively easy to explore model sensitivity to processes related to the nitrogen budget of the ETSP. Even though some spatial and temporal variations are missing compared with results from the global circulation models (Krishnamurthy et al., 2007, 2010; Zamora et al., 2010), we can efficiently diagnose the regional impacts at steady state. Stimulatory effects can be identified, respectively, between nitrogen fixation and water-column denitrification, phosphate regeneration and nitrogen fixation, phosphate regeneration and water-column denitrification, and atmospheric deposition and lateral NO_3^- transport (Fig. 4). Depressive effects occur between atmospheric deposition and nitrogen fixation, benthic denitrification and the lateral NO_3^- transport (Fig. 4). The model sensitivity to processes related to the nitrogen budget of the OMZ in the ETSP is illustrated in Fig. 7. The Nitrogen fixation rate can be enhanced by benthic denitrification, com-

BGD
12, 14441–14479, 2015

pensating for part of the NO_3^- loss. The stimulatory effect between nitrogen fixation and water-column denitrification can help to keep a fixed-N balance in the ocean. The extra fixed-N input by nitrogen deposition can be counteracted by decreased nitrogen fixation and partially removed by lateral flux. All of these local responses combined constitute a nitrogen-balancing mechanism in the ETSP. Even though anammox has been suggested as a possible major fixed-N loss in the water column of the ETSP (Lam et al., 2009; Kalvelage et al., 2013), both denitrification and anammox are ultimately driven by the flux of organic matter (Koeve and Kähler, 2010) and create a fixed-N deficit. Hence, the stimulatory effects between nitrogen fixation and fixed-N loss, and phosphate regeneration and fixed-N loss still apply even if anammox replaced water-column denitrification as the fixed-N loss pathway. Thus, the nitrogen-balancing mechanism in the ETSP should not depend on whether the fixed-N is lost through denitrification or anammox.

In the high-BD sensitivity experiment, our model domain turns into a NO_3^- sink (Fig. 4). The NO_3^- inventory in the ETSP is determined by nitrogen fixation, water-column denitrification, benthic denitrification and lateral NO_3^- flux. Since nitrogen fixation and water-column denitrification occur only in the surface ocean and the OMZ, which are included in our model domain, we cannot rule out that the ETSP including sedimentary denitrification is a NO_3^- sink, which is consistent with many model-derived or observational results (Ganachaud and Wunsch, 2002; Kalvelage et al., 2013). Extra phosphate input into the model domain via phosphate regeneration can increase water-column denitrification significantly due to the increase of EP from the surface ocean. However, phosphate regeneration alone can not turn our model domain into a NO_3^- sink, which corroborates that the water column of ETSP is net source of NO_3^-.

The remineralization rate of organic matter is thought to be reduced under anoxic conditions (Martin et al., 1987; Van Mooy et al., 2002), which results in more RRPOC reaching the sediments. According to the analysis of Bohlen et al. (2012), benthic denitrification is very sensitive to RRPOC, i.e., higher RRPOC results in higher benthic denitrification. Based on the findings that higher benthic denitrification can increase ni-

BGD
12, 14441–14479, 2015

trogen fixation, higher nitrogen fixation could result in higher water-column denitrification and the expansion of OMZs and finally a positive feedback between water-column and benthic denitrification. But this positive feedback is only observed in the configurations with phosphate input via phosphate regeneration, which indicates that PO_4^{3-} limitation could prevent this positive nitrogen loss feedback.

Appendix

It is known from laboratory experiments that diazotrophic phytoplankton can also utilize DIN for growth (e.g., Holl and Montoya, 2005). In contrast to our NF model where NF can only fix N_2 from the atmosphere, Schmittner et al. (2008) introduced a formulation to allow also NO_3^- uptake by diazotrophs. In Schmittner et al. (2008)'s model, nitrogen fixers preferentially use nitrate when available and cover only the residual N demand by N_2 fixation, denoted as facultative N_2-fixation. Thus, we explore the effect of facultative N_2-fixation on our model results with extra fixed-N input by nitrogen deposition.

Compared to results from the configurations in which NF can only fix N_2 (Fig. 3), both Phy and NF in the U-box are more robust to the extra nitrogen input via nitrogen deposition, for instance, Phy increases by 1.5 % (facultative N_2-fixation) vs. 2.9 % (obligate N_2 fixation), and NF decreases by 3.9 % (facultative N_2-fixation) vs. 10 % (obligate N_2 fixation). Again, the biogeochemical concentrations at steady state are relatively insensitive to nitrogen deposition (not shown).

There is a stronger negative feedback between nitrogen deposition and facultative N_2-fixation, since nitrogen fixation is reduced by about 21 % (facultative N_2-fixation) compared to 12 % (obligate N_2 fixation) (Fig. 8). The increased lateral fluxes of NO_3^- only account for about 21 % of the extra nitrogen input by nitrogen deposition (facultative N_2-fixation) compared to 50 % (obligate N_2 fixation) (Fig. 8). Thus, facultative N_2-fixation can adjust nitrogen fixation in response to nutrient concentrations in the surface boxes and control the magnitude of our model domain being a NO_3^- source.

BGD
12, 14441–14479, 2015

Author contributions. All co-authors jointly conceived and designed this study. B. Su performed all model simulations and data analysis. B. Su prepared the manuscript with contributions from all co-authors.

Acknowledgements. The authors wish to acknowledge funding from CSC (Chinese Scholarship Council), Sonderforschungsbereich 754 "Climate-Biogeochemistry Interaction in the Tropical Ocean" (www.sfb754.de) supported by the Deutsche Forschungsgemeinschaft, and the Cluster of Excellence "The Future Ocean", Kiel, Germany. The authors also wish to thank Wolfgang Koeve and Paul Kähler for the great help in improving this manuscript.

The article processing charges for this open-access publication were covered by a Research Centre of the Helmholtz Association.

References

Auguéres, A.-S. and Loreau, M.: Regulation of Redfield ratios in the deep ocean, Global Biogeochem. Cy., 29, 254–266, doi:10.1002/2014GB005066, 2015. 14443

Bakun, A. and Weeks, S. J.: The marine ecosystem off peru: what are the secrets of its fishery productivity and what might its future hold?, Prog. Oceanogr., 79, 290–299, 2008. 14443

Behrenfeld, M. J., Boss, E., Siegel, D. A., and Shea, D. M.: Carbon-based ocean productivity and phytoplankton physiology from space, Global Biogeochem. Cy., 19, 1–14, GB1006, doi:10.1029/2004GB002299, 2005. 14448, 14449, 14453

Berelson, W. M.: The flux of particulate organic carbon into the ocean interior: a comparison of four U.S. JGOFS regional studies, Oceanography, 14, 59–67, 2001. 14448

Bohlen, L., Dale, A. W., Sommer, S., Mosch, T., Hensen, C., Noffke, A., Scholz, F., and K. Wallmann: Benthic nitrogen cycling traversing the Peruvian oxygen minimum zone, Geochim. Cosmochim. Ac., 75, 6094–6111, 2011. 14444

Bohlen, L., Dale, A. W., and K. Wallmann: Simple transfer functions for calculating benthic fixed nitrogen losses and C : N : P regeneration ratios in global biogeochemical models, Global Biogeochem. Cy., 26, 1–16, GB3029, doi:10.1029/2011GB004198, 2012. 14443, 14447, 14449, 14459

BGD

12, 14441–14479, 2015

Brandes, J. A. and Devol, A. H.: A global marine-fixed nitrogen isotopic budget: Implications for holocene nitrogen cycling, Global Biogeochem. Cy., 16, 1–14, doi:10.1029/2001GB001856, 2002. 14443

Canfield, D. E.: Models of oxic respiration, denitrification and sulfate reduction in zones of coastal upwelling, Geochim. Cosmochim. Ac., 70, 5753–5765, doi:10.1016/j.gca.2006.07.023, 2006. 14444

Christensen, J. P., Murray, J. W., Devol, A., and Codispoti, L. A.: Denitrification in the continental shelf sediment has major impact on the oceanic nitrogen budget, Global Biogeochem. Cy., 1, 97–116, 1987. 14444

Clarke, L., Edmonds, J., Jacoby, H., Pitcher, H., Reilly, J., and Richels: Scenarios of Greenhouse Gas Emissions and Atmospheric Concentrations: Synthesis and Assessment Product 2.1a Report by the U.S. Climate Change Science Program and the Subcommittee on Global Change Research, Technical Report, Department of Energy, Office of Biological and Environmental Research, Washington, D.C., USA, 2007.

Codispoti, L. A.: An oceanic fixed nitrogen sink exceeding 400 Tg N a^{-1} vs the concept of homeostasis in the fixed-nitrogen inventory, Biogeosciences, 4, 233–253, doi:10.5194/bg-4-233-2007, 2007. 14443

Codispoti, L. A., Brandes, J., Christensen, J., Devol, A., Naqvi, S. W., Paerl, H., and Yoshinari, T.: The oceanic fixed nitrogen and nitrous oxide budgets: moving targets as we enter the anthropocene?, Sci. Mar., 65, 85–105, doi:10.3989/scimar.2001.65s285, 2001. 14443

Cornella, S. E., Jickells, T. D., Cape, J. N., Rowland, A. P., and Duce, R. A.: Organic nitrogen deposition on land and coastal environments: a review of methods and data, Atmos. Environ., 37, 2173–2191, doi:10.1016/S1352-2310(03)00133-X, 2003. 14445

Dentener, F., Drevet, J., Lamarque, J. F., Bey, I., Eickhout, B., Fiore, A. M., Hauglustaine, D., Horowitz, L. W., Krol, M., Kulshrestha, U. C., Lawrence, M., Galy-Lacaux, C., Rast, S., Shindell, D., Stevenson, D., Noije, T. V., Atherton, C., Bell, N., Bergman, D., Butler, T., Cofala, J., Collins, B., Doherty, R., Ellingsen, K., Galloway, J., Gauss, M., Montanaro, V., Müller, J. F., Pitari, G., Rodriguez, J., Sanderson, M., Solmon, F., Strahan, S., Schultz, M., Sudo, K., Szopa, S., and Wild, O.: Nitrogen and sulfur deposition on regional and global scales: a multimodel evaluation, Global Biogeochem. Cy., 20, 1–21, GB4003, doi:10.1029/2005GB002672, 2006. 14447, 14457

Deutsch, C., Gruber, N., Key, R. M., Sarmiento, J. L., and Ganachaud, A.: Denitrification and N_2 fixation in the Pacific Ocean, Global Biogeochem. Cy., 15, 483–506, 2001. 14445

BGD
12, 14441–14479, 2015

Deutsch, C., Sarmiento, J. L., Sigman, D. M., Gruber, N., and Dunne, J. P.: Spatial coupling of nitrogen inputs and losses in the ocean, Nature, 445, 163–167, 05392, doi:10.1038/nature05392, 2007. 14445, 14457

Devol, A. H.: Direct measurement of nitrogen gas fluxes from continental shelf sediments, Nature, 349, 319–321, 1991. 14444

DeVries, T., Deutsch, C., Primeau, F., Chang, B., and Devol, A.: Global rates of water-column denitrification derived from nitrogen gas measurements, Nature, 5, 547–550, doi:10.1038/NGEO1515, 2012. 14443

Duarte, C. M., Dachs, J., Llabrés, M., Alonso-Laita, P., Gasol, J. M., Tovar-Sánchez, A., nudo Wilhemy, S. S., and Agustí, S.: Aerosol inputs enhance new production in the subtropical northeast Atlantic, J. Geophys. Res., 111, 1–8, G04006, 2006. 14445

Duce, R. A.: The impact of atmospheric nitrogen, phosphorus, and iron species on marine biological productivity, in: The Role of Air–Sea Exchange in Geochemical Cycling, vol. 185 of NATO ASI Series, edited by: P. Buat-Ménard, Springer, New York, 497–529, 1986. 14444

Duce, R. A., Liss, P. S., Merrill, J. T., Atlas, E. L., Buat-Menard, P., Hicks, B. B., Miller, J. M., Prospero, J. M., Arimoto, R., Church, T. M., Ellis, W., Galloway, J. N., Hansen, L., Jickells, T. D., Knap, A. H., Reinhardt, K. H., Schneider, B., Soudine, A., Tokos, J. J., Tsunogai, S., Wollast, R., and Zhou, M.: The atmospheric input of trace species to the world ocean, Global Biogeochem. Cy., 5, 193–259, 1991. 14444, 14447

Duce, R. A., LaRoche, J., Altieri, K., Arrigo, K. R., Baker, A. R., Capone, D. G., Cornell, S., Dentener, F., Galloway, J., Ganeshram, R. S., Geider, R. J., Jickells, T., Kuypers, M. M., Langlois, R., Liss, P. S., Liu, S. M., Middelburg, J. J., Moore, C. M., Nickovic, S., Oschlies, A., Pedersen, T., Prospero, J., Schlitzer, R., Seitzinger, S., Sorensen, L. L., Uematsu, M., Ulloa, O., Voss, M., Ward, B., and Zamora, L.: Impacts of atmospheric anthropogenic nitrogen on the open ocean, Science, 320, 893–897, 5878, 2008. 14443, 14444, 14445, 14447, 14457

Dunne, J. P., Armstrong, R. A., Gnanadesikan, A., and Sarmiento, J. L.: Empirical and mechanistic models for the particle export ratio, Global Biogeochem. Cy., 19, 1–16, GB4026, doi:10.1029/2004GB002390, 2005. 14449

Eugster, O. and Gruber, N.: A probabilistic estimate of global marine N-fixation and denitrification, Global Biogeochem. Cy., 26, 1–15, GB4013, doi:10.1029/2012GB004300, 2012. 14443

Falkowski, P. G., Barber, R. T., and Smetacek, V.: Biogeochemical Controls and Feedbacks on Ocean Primary Production, Science, 281, 200–206, 1998. 14443

BGD
12, 14441–14479, 2015

Flögel, S., Wallmann, K., Poulsen, C. J., Zhou, J., Oschlies, A., Voigt, S., and Kuhnt, W.: Simulating the biogeochemical effects of volcanic CO_2 degassing on the oxygen-state of the deep ocean during the Cenomanian/Turonian Anoxic Event (OAE2), Earth Planet. Sc. Lett., 305, 371–384, 2011. 14450

Ganachaud, A. and Wunsch, C.: Oceanic nutrients and oxygen transports and bounds on export production during the world ocean circulation experiment, Global Biogeochem. Cy., 16, 1–14, doi:10.1029/2000GB001333, 2002. 14459

Garcia, H. E., Locarnini, R. A., Boyer, T. P., Antonov, J. I., Baranova, O. K., Zweng, M. M., and Johnson, D. R.: Volume 3: Dissolved oxygen, apparent oxygen utilization, and oxygen saturation, in: World Ocean Atlas 2009, edited by: Levitus, S., NOAA Atlas NESDIS 70, U.S. Government Printing Office, Washington, D.C., p. 344, 2010a. 14449

Garcia, H. E., Locarnini, R. A., Boyer, T. P., Antonov, J. I., Zweng, M. M., Baranova, O. K., and Johnson, D. R.: Volume 4: Nutrients (phosphate, nitrate, silicate), in: World Ocean Atlas 2009, edited by: Levitus, S., NOAA Atlas NESDIS 71, U.S. Government Printing Office, Washington, D.C., p. 398., 2010b. 14449

Großkopf, T., Mohr, W., Baustian, T., Schunck, H., Gill, D., Kuypers, M. M. M., Lavik, G., Schmitz, R. A., Wallace, D. W. R., and LaRoche, J.: Doubling of marine dinitrogen-fixation rates based on direct measurements, Nature, 488, 361–364, 2012. 14443

Gruber, N.: The dynamics of the marine nitrogen cycle and its influence on atmospheric CO_2 variations, in: The Ocean Carbon Cycle and Climate, vol. 40 of NATO Science Series, chapt. 4, edited by: Follows, M. and Oguz, T., Kluwer Academic, P.O. Box 17,3300 AA Dordrecht, the Netherlands, 97–148, 2004. 14442, 14443

Gruber, N. and Sarmiento, J. L.: Large-scale biogeochemical-physical interactions in elemental cycles, in: Biogeochemical/Physical Interactions in Elemental Cycles, vol. 12 of The Sea, chapt. 9, edited by: Robinson, A. R., Macarthy, J. J., Rothschild, B. J., J. Wiley and Sons, Harward University Press, 337–399, New York, 2002. 14443

Holl, C. M. and Montoya, J. P.: Interactions between nitrate uptake and nitrogen fixation in continuous cultures of the marine diazotroph *Trichodesmium* (Cyanobacteria), J. Phycol., 41, 1178–1183, doi:10.1111/j.1529-8817.2005.00146.x, 2005. 14460

Kalvelage, T., Lavik, G., Lam, P., Contreras, S., Arteaga, L., Löscher, C. R., Oschlies, A., Paulmier, A., Stramma, L., and Kuypers, M. M. M.: Nitrogen cycling driven by organic matter export in the South Pacific oxygen minimum zone, Nat. Geosci., 6, 228–234, doi:10.1038/NGEO1739, 2013. 14444, 14459

BGD
12, 14441–14479, 2015

Kasai, A., Kimura, S., Nakata, H., and Okazaki, Y.: Entrainment of coastal water into a frontal eddy of the kuroshio and its biological significance, J. Marine Syst., 37, 185–198, 2002. 14443

Koeve, W. and Kähler, P.: Heterotrophic denitrification vs. autotrophic anammox – quantifying collateral effects on the oceanic carbon cycle, Biogeosciences, 7, 2327–2337, doi:10.5194/bg-7-2327-2010, 2010. 14444, 14459

Krishnamurthy, A., Moore, J. K., Zender, C. S., and Luo, C.: Effects of atmospheric inorganic nitrogen deposition on ocean biogeochemistry, J. Geophys. Res., 112, 1–10, G02019, doi:10.1029/2006JG000334, 2007. 14444, 14445, 14457, 14458

Krishnamurthy, A., Moore, J. K., Mahowald, N., Luo, C., Doney, S. C., Lindsay, K., and Zender, C. S.: Impacts of increasing anthropogenic soluble iron and nitrogen deposition on ocean biogeochemistry, Global Biogeochem. Cy., 23, 1–15, GB3016, doi:10.1029/2008GB003440, 2009. 14457

Krishnamurthy, A., Moore, J. K., Mahowald, N., Luo, C., and Zender, C. S.: Impacts of atmospheric nutrient inputs on marine biogeochemistry, J. Geophys. Res., 115, 1–13, G01006, doi:10.1029/2009JG001115, 2010. 14444, 14457, 14458

Lam, P., Lavika, G., Jensena, M. M., van de Vossenberg, J., Schmidb, M., Woebkena, D., Gutiérrezc, D., Amanna, R., Jettenb, M. S. M., and Kuypersa, M. M. M.: Revising the nitrogen cycle in the Peruvian oxygen minimum zone, P. Natl. Acad. Sci. USA, 106, 4752–4757, doi:10.1073/pnas.0812444106, 2009. 14444, 14459

Lamarque, J.-F., Kyle, G. P., Meinshausen, M., Riahi, K., Smith, S. J., van Vuuren, D. P., Conley, A. J., and Vitt, F.: Global and regional evolution of short-lived radiatively-active gases and aerosols in the Representative Concentration Pathways, Climatic Change, 109, 191–121, doi:10.1007/s10584-011-0155-0, 2011. 14447, 14469

Landolfi, A., Dietze, H., Koeve, W., and Oschlies, A.: Overlooked runaway feedback in the marine nitrogen cycle: the vicious cycle, Biogeosciences, 10, 1351–1363, doi:10.5194/bg-10-1351-2013, 2013. 14445

Locarnini, R. A., Mishonov, A. V., Antonov, J. I., Boyer, T. P., Garcia, H. E., Baranova, O. K., Zweng, M. M., and Johnson, D. R.: Volume 1: Temperature, in: World Ocean Atlas 2009, NOAA Atlas NESDIS 68, edited by: Levitus, S., U.S. Government Printing Office, Washington, D.C., p. 184, 2010. 14449

Mahowald, N., Jickells, T. D., Baker, A. R., Artaxo, P., Benitez-Nelson, C. R., Bergametti, G., Bond, T. C., Chen, Y., Cohen, D. D., Herut, B., Kubilay, N., Losno, R., Luo, C., Maen-

BGD
12, 14441–14479, 2015

haut, W., McGee, K. A., Okin, G. S., Siefert, R. L., and Tsukuda, S.: Global distribution of atmospheric phosphorus sources, concentrations and deposition rates, and anthropogenic impacts, Global Biogeochem. Cy., 22, 1–19, GB4026, doi:10.1029/2008GB003240, 2008. 14447

Martin, J. H., Knauer, G. A., Karl, D. M., and Broenkow, W. W.: VERTEX: carbon cycling in the northeast Pacific, Deep-Sea Res., 34, 267–285, 1987. 14448, 14449, 14451, 14459

Moore, C. M., Mills, M. M., Arrigo, K. R., Berman-Frank, I., Bopp, L., Boyd, P. W., Galbraith, E. D., Geider, R. J., Guieu, C., Jaccard, S. L., Jickells, T. D., LaRoche, J., Lenton, T. M., Mahowald, N. M., Marañón, E., Marinov, I., Moore, J. K., Nakatsuka, T., Oschlies, A., Saito, M. A., Thingstad, T. F., Tsuda, A., and Ulloa, O.: Processes and patterns of oceanic nutrient limitation, Nature Geosci., 6, 701–710, doi:10.1038/NGEO1765, 2013. 14443

Moore, J. K. and Braucher, O.: Sedimentary and mineral dust sources of dissolved iron to the world ocean, Biogeosciences, 5, 631–656, doi:10.5194/bg-5-631-2008, 2008. 14443

Moss, R. H., Edmonds, J. A., Hibbard, K. A., Manning, M. R., Rose, S. K., van Vuuren, D. P., Carter, T. R., Emori, S., Kainuma, M., Kram, T., Meehl, G. A., Mitchell, J. F. B., Nakicenovic, N., Riahi, K., Smith, S. J., Stouffer, R. J., Thomson, A. M., Weyant, J. P., and Wilbanks, T. J.: The next generation of scenarios for climate change research and assessment, Nature, 463, 747–756, doi:10.1038/nature08823, 2010.

Mouriño-Carballido, B., Pahlow, M., and Oschlies, A.: High sensitivity of ultra-oligotrophic marine ecosystems to atmospheric nitrogen deposition, Geophys. Res. Lett., 39, 1–6, L05601, doi:10.1029/2011GL050606, 2012. 14444

Okin, G. S., Baker, A. R., Tegen, I., Mahowald, N. M., Dentener, F. J., Duce, R. A., Galloway, J. N., Hunter, K., Kanakidou, M., Kubilay, N., Prospero, J. M., Sarin, M., Surapipith, V., Uematsu, M., and Zhu, T.: Impacts of atmospheric nutrient deposition on marine productivity: roles of nitrogen, phosphorus, and iron, Global Biogeochem. Cy., 25, 1–10, GB2022, 2011. 14442, 14444

Paerl, H. W. and Whitall, D. R.: Anthropogenically-derived atmospheric nitrogen deposition, marine eutrophication and harmful algal bloom expansion: is there a link?, Ambio, 28, 307–311, 1999. 14445

Reay, D. S., Dentener, F., Smith, P., Grace, J., and Feely, R. A.: Global nitrogen depisition and carbon sinks, Nature Geosci., 1, 430–437, 2008. 14457

Schmittner, A., Oschlies, A., Matthews, H. D., and Galbraith, E. D.: Future changes in climate, ocean circulation, ecosystems, and biogeochemical cycling simulated for a business-

BGD
12, 14441–14479, 2015

as-usual CO_2 emission scenario until year 4000 AD, Global Biogeochem. Cy., 22, 1–21, GB1013, doi:10.1029/2007GB002953, 2008. 14460
Seitzinger, S. P. and Sanders, R. W.: Atmospheric inputs of dissolved organic nitrogen stimulate estuarine bacteria and phytoplankton, Limnol. Oceanogr., 44, 721–730, 1999. 14445
Slomp, C. P. and Van Cappellen, P.: The global marine phosphorus cycle: sensitivity to oceanic circulation, Biogeosciences, 4, 155–171, doi:10.5194/bg-4-155-2007, 2007. 14443
Somes, C. J., Oschlies, A., and Schmittner, A.: Isotopic constraints on the pre-industrial oceanic nitrogen budget, Biogeosciences, 10, 5889–5910, doi:10.5194/bg-10-5889-2013, 2013. 14445, 14457
Su, B., Pahlow, M., Wagner, H., and Oschlies, A.: What prevents nitrogen depletion in the oxygen minimum zone of the eastern tropical South Pacific?, Biogeosciences, 12, 1113–1130, doi:10.5194/bg-12-1113-2015, 2015. 14443, 14445, 14446, 14454
Tyrrell, T.: The relative influences of nitrogen and phosphorus on oceanic primary production, Nature, 400, 525–531, 1999. 14443
Van Cappellen, P. and Ingall, E. D.: Benthic phosphorus regeneration, net primary production, and ocean anoxia: a model of the coupled marine biogeochemical cycles of carbon and phosphorus, Paleoceanography, 9, 677–692, 1994. 14444, 14445, 14458
Van Mooy, B. A. S., Keil, R. G., and Devol, A. H.: Impact of suboxia on sinking particulate organic carbon: enhanced carbon flux and preferential degradation of amino acids via denitrification, Geochim. Cosmochim. Ac., 66, 457–467, doi:10.1016/S0016-7037(01)00787-6, 2002. 14448, 14451, 14459
Wallmann, K.: Feedbacks between oceanic redox states and marine productivity: a model perspective focused on benthic phosphorus cycling, Global Biogeochem. Cy., 17, 1–10, 2003. 14444
Wallmann, K.: Phosphorus imbalance in the global Ocean, Global Biogeochem. Cy., 24, 1–12, GB4030, doi:10.1029/2009GB003643, 2010. 14443, 14444, 14450, 14451, 14458
Ward, B. B., Devol, A. H., Rich, J. J., Chang, B. X., Bulow, S. E., Naik, H., Pratihary, A., and Jayakumar, A.: Denitrification as the dominant nitrogen loss process in the Arabian Sea, Nature, 461, 78–81, doi:10.1038/nature08276, 2009. 14444
Warneck, P.: Chemistry of the Natural Atmosphere, vol. 71 of International Geophysics Series, Elsevier, New York, 1988. 14445

BGD
12, 14441–14479, 2015

Wise, M., Calvin, K., Thomson, A., Clarke, L., Bond-Lamberty, B., Sands, R., Smith, S. J., Janetos, A., and Edmonds, J.: Implications of limiting CO_2 concentrations for land use and energy, Science, 324, 1183–1189, doi:10.1126/science.1168475, 2009.

Zamora, L. M., Landolfi, A., Oschlies, A., Hansell, D. A., Dietze, H., and Dentener, F.: Atmospheric deposition of nutrients and excess N formation in the North Atlantic, Biogeosciences, 7, 777–793, doi:10.5194/bg-7-777-2010, 2010. 14457, 14458

Zamora, L. M., Prospero, J. M., and Hansell, D. A.: Organic nitrogen in aerosols and precipitation at Barbados and Miami: implications regarding sources, transport and deposition to the western subtropical North Atlantic, J. Geophys. Res., 116, 1–17, D20309, doi:10.1029/2011JD015660, 2011. 14445

BGD
12, 14441–14479, 2015

Table 1. Summary of model configurations. Model BD and Data BD represent model- and data-based benthic denitrification, respectively. Model PR and Data PR are model- and data-based benthic phosphate regeneration, respectively. N-DEP represents the atmospheric nitrogen input into the surface ocean according to the estimate by Lamarque et al. (2011).

Configuration	Process				
	Model BD	Data BD	Model PR	Data PR	N-DEP
Control					
N-DEP					+
MBD	+				
MPR			+		
DBD		+			
DPR				+	
Synthesis configuration					
MBD+MPR (Syn1)	+		+		
DBD+DPR (Syn2)		+		+	
MBD+MPR+N-DEP (Syn3)	+		+		+
DBD+DPR+N-DEP (Syn4)		+		+	+

+ indicates that the process is included.

BGD
12, 14441–14479, 2015

Table 2. Sediment percentage and average Martin curve value used for the model-based estimation of benthic denitrification. "Sediment percentage" is the percentage of the surface areas of the UM and D boxes in contact with the sediment; "Average Martin curve value" represents the average of Martin curve fractions of export production reaching the sediment for each grid point of the topography data.

	Sediment percentage (SD, %)	Average Martin curve value (AMC, %)
UM box	0.81	53.04
D box	2.25	12.51

BGD
12, 14441–14479, 2015

Table 3. Fixed-N loss via benthic denitrification (BD) and phosphate release via phosphate regeneration (PR) in the UM and D boxes. High-BD indicates that the full sediment of the D box is included to estimate NO_3^- loss via benthic denitrification and phosphate release via phosphate regeneration. These values are estimated from Aqua-Modis satellite data.

	NPP ($mg\,C\,m^{-2}\,day^{-1}$)	Rain rate	BD ($Tg\,N\,yr^{-1}$)	PR ($Tg\,P\,yr^{-1}$)
UM	1374.7	148.4	0.17	0.058
D	873.9	12.2	0.82	0.056
D (high-BD/PR)	873.9	12.2	8.8	0.56

BGD
12, 14441–14479, 2015

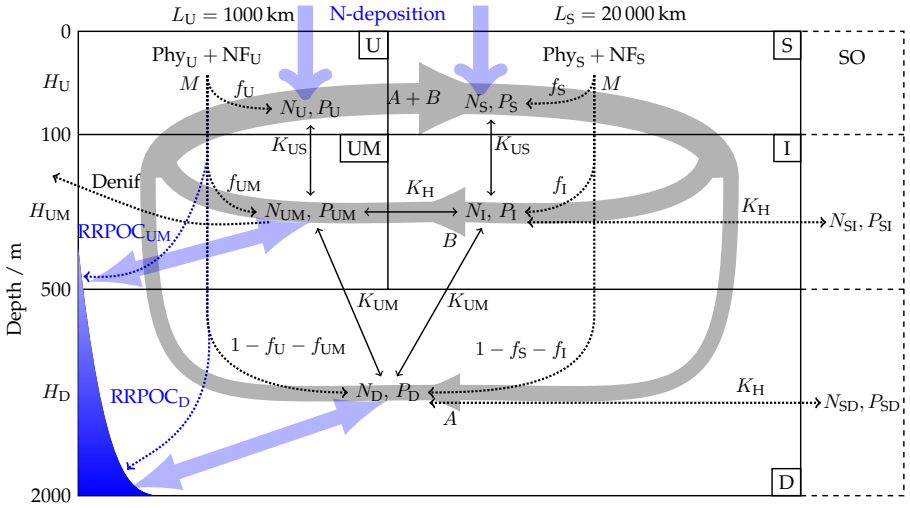

Figure 1. Model structure. The model domain comprises five boxes representing the top 100 m of an upwelling region (U), the underlying oxygen minimum zone (UM), and an adjacent open-ocean basin divided into a surface (S) and an intermediate-depth box (I). A deep box (D) underlies both the upwelling region and the open ocean. The large-scale circulation is represented by deep (A) and shallow (B) convection (thick grey lines). Mixing between boxes is implemented via mixing coefficients (K). Remineralisation derived from primary production by ordinary (Phy) and diazotrophic (NF) phytoplankton in the surface boxes consumes oxygen. Under anoxic conditions remineralisation is fueled by anaerobic remineralization (Denif). In the configuration employed in this study, the model domain exchanges nutrients and oxygen with the Southern Ocean (right, denoted as "SO"). Nitrogen deposition and benthic remineralization are included additionally to represent their influence on the local water-column nutrient concentrations (thick light blue arrows).

BGD
12, 14441–14479, 2015

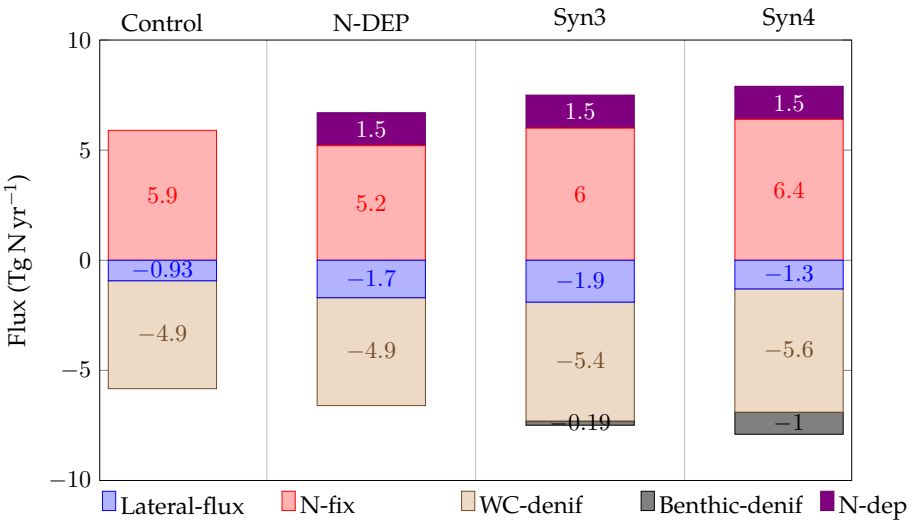

Figure 2. Nitrogen fluxes after including atmospheric nitrogen deposition in the control, Syn3 and Syn4 configurations defined in Table 1. Lateral-flux identifies the nitrogen efflux or influx through the southern boundary; N-fix represents the nitrogen fixation rate by NF; WC-denif is water-column denitrification; N-dep is the nitrogen input into surface ocean via nitrogen deposition.

BGD
12, 14441–14479, 2015

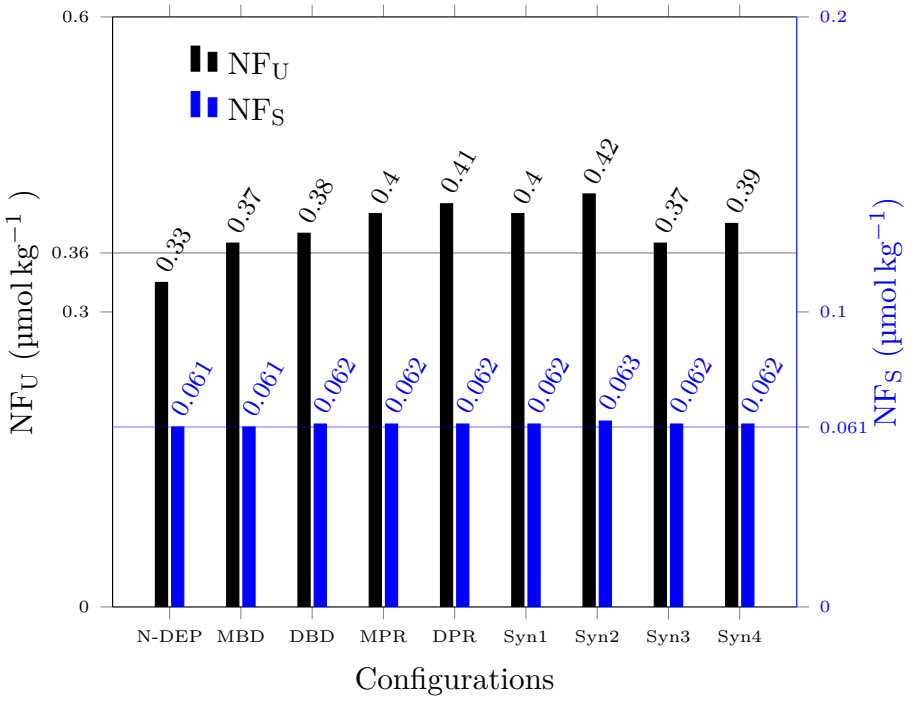

Figure 3. Sensitivity of simulated steady-state concentrations of nitrogen fixers NF_U and NF_S in the U and S boxes respectively. Horizontal grey and light blue lines represent the NF_U and NF_S concentrations in the control configuration respectively. Syn1, Syn2, Syn3 and Syn4 denote the "MBD + MPR", "DBD + DPR", "MBD + MPR + N-DEP", and "DBD + DPR + N-DEP" synthesis configurations defined in Table 1.

BGD
12, 14441–14479, 2015

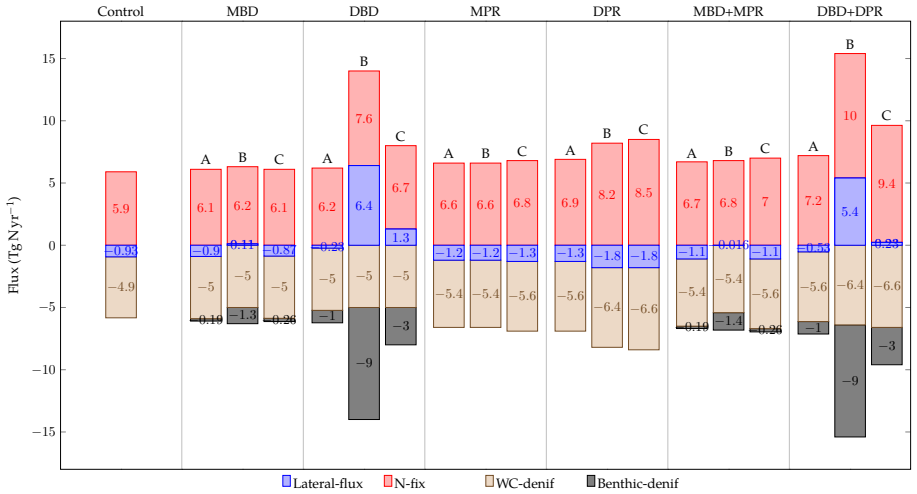

Figure 4. Nitrogen fluxes after including benthic denitrification or/and phosphate regeneration. Lateral-flux identifies the nitrogen efflux or influx through the southern boundary; N-fix represents the nitrogen fixation rate by NF; WC-denif is water-column denitrification; Benthic-denif represents the fixed-N loss via benthic denitrification in the model domain. Bar labels: A, main experiments; B, sensitivity experiments with high-BD; C, sensitivity experiments with Martin Curve exponent b = 0.4.

BGD
12, 14441–14479, 2015

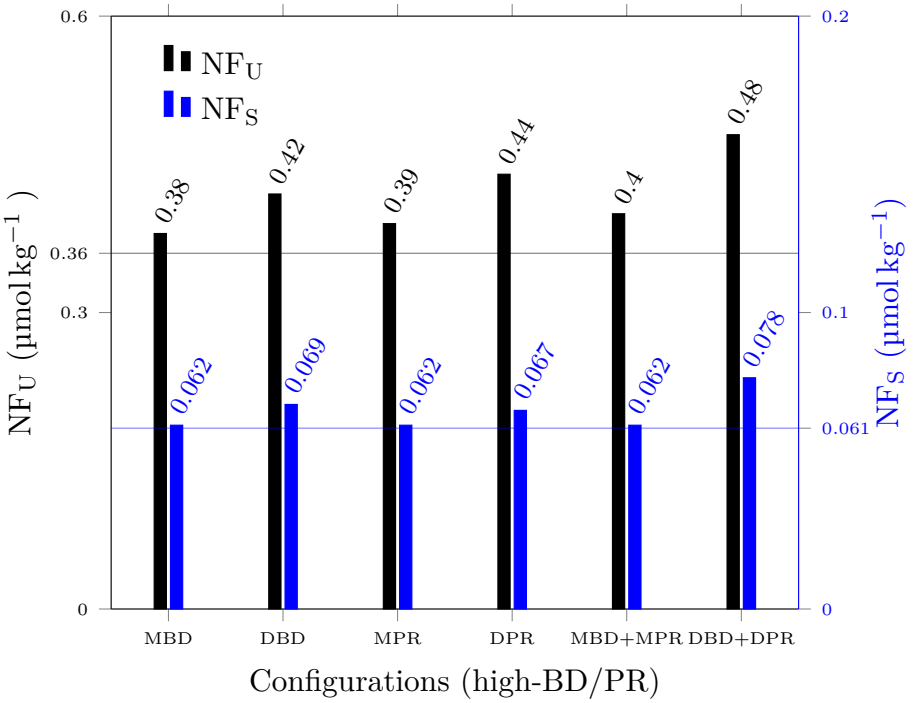

Figure 5. Sensitivity of simulated steady-state concentrations of nitrogen fixers (NF_U and NF_S) in the U and S boxes respectively after incorporating high-BD and high-PR. Horizontal grey and light blue lines represent the NF_U and NF_S concentrations in the control configuration.

BGD
12, 14441–14479, 2015

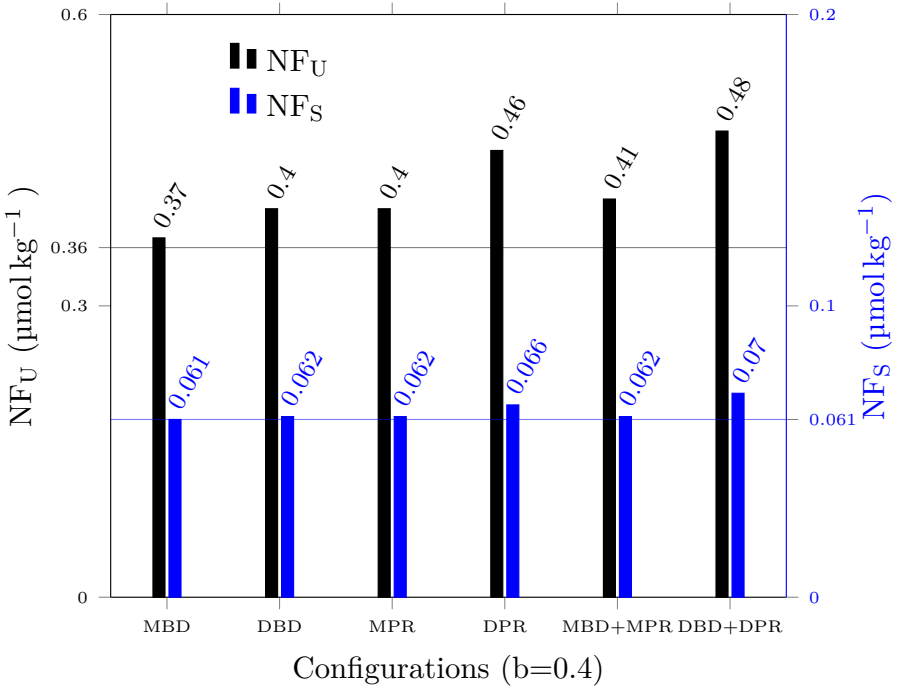

Figure 6. Sensitivity of simulated steady-state concentrations of nitrogen fixers (NF_U and NF_S) in the U and S boxes respectively after applying $b = 0.4$ for Eq. (2). Horizontal grey and light blue lines represent the NF_U and NF_S concentrations in the control configuration.

BGD
12, 14441–14479, 2015

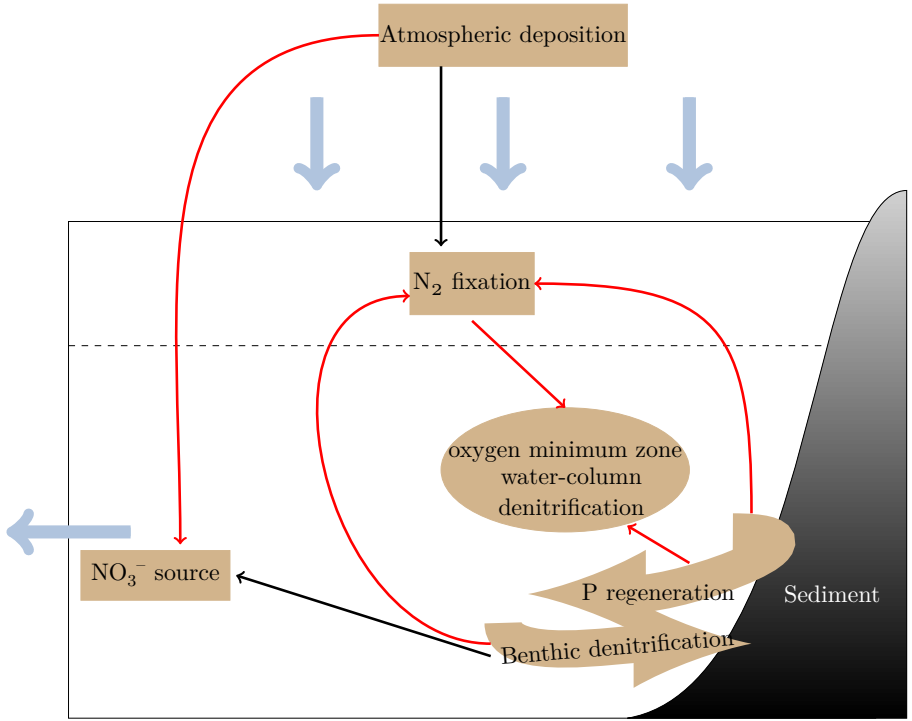

Figure 7. Schematic of the model sensitivity to different processes related to the nitrogen budget of the ETSP. The red solid lines present stimulatory effects, and the black solid lines represent depressive effects.

BGD
12, 14441–14479, 2015

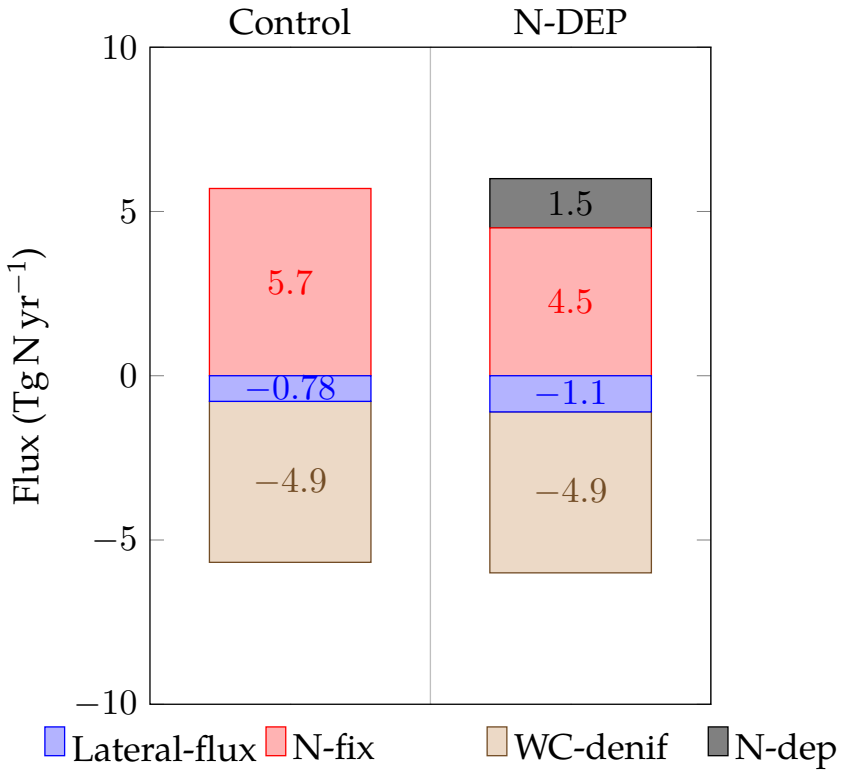

Figure 8. Nitrogen fluxes after including atmospheric nitrogen deposition in the model with facultative N_2-fixation. Labels are the same as those in Fig. 2.

BGD
12, 14441–14479, 2015